



HAL
open science

A Portable Device Performing Continuous Impedance Spectroscopy for Skin Conductivity

Bertrand Massot, Emeric Desmazure, Amalric Montalibet, Eric Mcadams,
Claudine Gehin

► **To cite this version:**

Bertrand Massot, Emeric Desmazure, Amalric Montalibet, Eric Mcadams, Claudine Gehin. A Portable Device Performing Continuous Impedance Spectroscopy for Skin Conductivity. IEEE Sensors Journal, 2024, pp.1-1. 10.1109/JSEN.2024.3485187 . hal-04788347

HAL Id: hal-04788347

<https://hal.science/hal-04788347v1>

Submitted on 18 Nov 2024

HAL is a multi-disciplinary open access archive for the deposit and dissemination of scientific research documents, whether they are published or not. The documents may come from teaching and research institutions in France or abroad, or from public or private research centers.

L'archive ouverte pluridisciplinaire **HAL**, est destinée au dépôt et à la diffusion de documents scientifiques de niveau recherche, publiés ou non, émanant des établissements d'enseignement et de recherche français ou étrangers, des laboratoires publics ou privés.



Distributed under a Creative Commons Attribution 4.0 International License

A Portable Device Performing Continuous Impedance Spectroscopy for Skin Conductivity

Bertrand Massot, Emeric Desmazure, Amalric Montalibet, Eric McAdams and Claudine Gehin

Abstract—Electrodermal activity is widely used in psychophysiological studies to quantify emotional responsiveness and stress. Existing devices typically assess skin conductivity using either constant current/voltage or a fixed-frequency excitation. However, skin behaves like a complex impedance system which is frequency dependent, but single-frequency methods only produce a single conductivity value. We propose a method to assess skin impedance at multiple frequencies simultaneously and continuously to observe temporal changes of the impedance at each frequency for the improved analysis of electrodermal activity. Furthermore, we present an implementation of this method in a wearable device to highlight its performances. We achieved the measurement of 16 frequencies simultaneously within the range 10 Hz – 1000 Hz at a rate of 8 samples per second. The device was evaluated using static impedances made from discrete electronic components and demonstrated an average error of 1.9%. An *in vivo* experiment was conducted on seven volunteers resting for 30 minutes. Measurements were taken consecutively with our device and the Sciospec ISX-3 at the same body location, without removing the electrodes, when electrodermal activity was minimal. The average difference between the two instruments on living tissues was 3.8%. Performing continuously impedance spectroscopy could enable a more robust and a more universal way to quantify electrodermal activity. Additionally having a complete spectrum of impedance may help improve the specificity of the analysis of electrodermal activity by better differentiating between sweat gland activity and changes in the electrode/skin interface using equivalent circuit modeling.

Index Terms—electrodermal activity, skin conductivity, impedance spectroscopy, instrumentation, wearable sensors.

I. INTRODUCTION

ELECTRODERMAL activity (EDA) encompasses all the electrical phenomena which can occur through the skin, such as electrical potential, current or impedance variations [1], which are primarily caused by the activity of sweat glands on the soles of the feet and the palms of the hands [2, p. 2], [3, p. 449]. These particular populations of eccrine glands are specifically innervated by the sympathetic branch of the autonomic nervous system, and consequently their secretion of sweat is directly related to the activation of the sympathetic nervous system [4], [5]. Through the measurement of electrical changes induced by the amount of sweat within the ducts, EDA is generally used within the frame of psychophysiological studies for the objectivation of cognitive and emotional processes, affective computing, and the investigation of psychopathologies such as anxiety, bipolar disorder, etc. [6]–[8] EDA is commonly assessed by measuring the changes in the skin's electrical potentials and conductivity induced by the activity of sweat glands. Intermittent secretions of sweat lead to rapid increases in conductivity known as Skin Conductance Responses (SCRs, or "phasic responses"), and tend to raise the average level of the skin's conductivity, termed the Skin Conductance Level (SCL, or "tonic level") [9], [10]. In contrast, progressive skin evaporation and partial

reabsorption by the tissues result in the gradual reduction of SCL. Thus, electrical conductivity of skin serves as a rapid and responsive indicator of sympathetic nervous system activity. From a very early stage, the skin's conductivity has been measured by applying a constant voltage across two electrodes placed on the palm or by injecting constant current through the electrodes [8], [11]. By measuring the resulting current (when applying voltage) or the difference in potential (when injecting current), it is possible using Ohm's law to deduce the electrical resistance or conductance. In the early works on EDA, it was also suggested, and in some cases tested that EDA could be measured using AC current / voltage at a fixed frequency instead of constant DC stimulation [12], [13]. Despite the additional indicators that this method furnishes (such as phase difference between voltage and current), it has not been as extensively used nor studied compared to the classical analysis of magnitude changes. Nonetheless, modern instruments measuring EDA implement AC voltage excitation to derive impedance magnitudes at the frequency of excitation [14]. In actual fact, the variety of methods employed in the electronics for the measurement of EDA is one of the major drawbacks in the analysis and comparison of the acquired signals. While the detection of SCRs is a time/event related analysis, which is independent of the method of measurement, the amplitudes of SCL and SCRs are directly biased by the magnitude and the frequency of the excitation signal. Another extrinsic factor of paramount importance influencing EDA measurement is the type of electrodes used, which directly impacts SCL over time and can lead to misinterpretations of short- and long-term variations. Skin conductivity is measured using either a 2- or 3-electrode configuration. In both cases,

This paper was submitted for review on April 2024. This work was supported in part by the French National Research Agency (ANR) under the grant ANR-22-CE31-0023-03.

B. Massot, E. Desmazure, A. Montalibet, E. McAdams and C. Gehin are with INSA Lyon, CNRS, Ecole Centrale de Lyon, Université Claude Bernard Lyon 1, CPE Lyon, INL, UMR5270, 69100 Villeurbanne, France (e-mail: bertrand.massot@insa-lyon.fr).

the electrode-skin interface is treated as a complex impedance within the measurement loop, in series with the living tissues, as depicted in established electrical behavior models [3], [15]. A significant study by Tronstad et al. demonstrated that variations in the electrode-skin interface over time could result in erroneous interpretations of SCL due to long-term impedance fluctuations and, in some cases, even inverted SCRs depending on the type of gel used with the electrodes [16].

In 2012, general recommendations were published to guide researchers when measuring and presenting results of EDA data [17]. According to those recommendations, when using DC measurements, a voltage in the order of 0.5 V should be applied. For AC measurements, a constant magnitude of 0.5 V is also recommended, and this method has the benefit of strongly reducing the so-called polarisation of electrodes compared with DC measurements. Regarding electrodes, disposable Ag/AgCl electrodes covered with solid hydrogel are the most recommended, due to their benefit compared to other types of electrodes (dry electrodes or wet-gelled electrodes) commonly used when measuring bioelectrical signals [14], [16].

In 2019, a consistent and systematic review of measurement methods was compiled and shows that a DC voltage source is the most common approach in psychophysiological applications. This is mainly due to the simplicity of the associated electronics, despite the strong disadvantages of this method regarding the influence of the electrodes' electrical properties on the measurement [18]. In addition to these two publications, a recent review by Tronstad et al. also states that there is a lack of studies regarding the way the skin's impedance changes with varying measurement frequencies when using an AC source [19]. According to Boucsein, switching from DC- to AC recording would lead to methodological progress in EDA measurement [2, p. 257].

Consequently, and also based on general knowledge regarding bioimpedance measurements in living tissues, measuring skin conductance using either DC or fixed-frequency AC stimulation provides only a very limited view of the underlying electrical changes that constitute EDA. Martinsen and Heiskanen emphasize that the AC method also raises the question of which frequency to measure if using a single frequency [3, p. 420]. As such, acquiring impedance over a range of optimally chosen frequencies simultaneously (i.e. performing an electrical impedance spectroscopic measurement) could help to better identify and highlight the impedance's changes that are most specific and sensitive to the activity of sweat glands; and better isolate this activity from the influence of skin-electrode interface. The actual advantages offered by multi-frequency results remain to be confirmed, and further studies are needed to analyze signals obtained under various electrode types and experimental conditions to determine the validity of the proposed hypotheses. In any case, at a minimum, this method will allow for modeling the complex impedance measured through the use of fitting tools and, most importantly, observing its temporal variations. As further described in the next section, impedance spectroscopy is a powerful technique in analysing biological tissue composition, and could bring new insights regarding tissue modelisation within the frame

of EDA. To achieve this goal, we designed and produced a portable electronic system capable of continuous impedance spectroscopy, suited for measuring EDA.

In section II, we present the principles of the measurement technique as well as the requirements for adapting impedance spectroscopy to EDA. In section III, we describe how we implemented real-time impedance spectroscopy within a miniaturised and portable electronic system with wireless communication. Section IV presents results of measurements on static electrical models as well as in-vivo measurements to demonstrate the ability of our system to perform impedance spectroscopy for the acquisition of EDA in real life experimental setups. Finally, we discuss in section V the benefits and limitations of this method and its proposed implementation within this electronic system.

II. PRINCIPLES

A. Impedance spectroscopy

Impedance spectroscopy basically consists in measuring the impedance of an unknown electrical load at multiple frequencies, rather than using DC current (which measures the resistance only), or using AC current at a single frequency. More specifically, impedance spectroscopy for bioimpedance measurements aims at providing real/imaginary or magnitude/phase values of a complex impedance over a specific range of frequencies to enhance the understanding of the underlying electrical behaviour of the tissue of interest.

The most common application for this method is to analyse the composition of biological tissues [20], [21]. For example, Body Impedance Analysers (BIA) can derive body composition parameters, such as percentage water or fat quantities, from the measurement of the whole-body impedance, by placing electrodes on hands and/or feet. In such applications, the target impedance lies within subcutaneous tissues, and hence the impedance is measured using a 4-electrode topology [22]. Furthermore, throughout the entire measurement duration, the target impedance can be considered constant because tissue composition undergoes relatively slow variations compared to the acquisition time. Thus, impedance values for each frequency do not need to be evaluated simultaneously and continuously, which is why most BIAs produce impedance spectroscopy by performing impedance measurements at one frequency at a time, and sweeping over the frequency range for a fixed number of points. Consequently, obtaining the entire impedance spectroscopy may take several seconds, particularly when evaluating low frequencies (< 1 kHz), which is incompatible with nonstationary electrical characteristics.

However, in the case of EDA, signals exhibit lower time-constant / faster variations, typically in the order of a second or less. SCRs are especially short, transient events whose duration is usually in the order of 2 s [2]. For the detection and analysis of SCRs, it is thus generally recommended to have a sample rate greater than 5 samples per second to preserve the relevant EDA signal information [19]. In consequence, if one seeks to obtain several complex impedance spectra per second over the range of frequencies of interest for EDA, this cannot be achieved using classical, commercially-available body impedance analysers. In the literature, several

methods have been proposed to assess impedance at multiple frequencies simultaneously at a high rate, specifically higher than one sample per second per frequency. One traditional approach involves the use of lock-in amplifiers, which enable precise measurement of multiple frequencies simultaneously [23]. However, this method requires as many lock-in amplifiers as there are frequencies to be measured, resulting in significantly larger electronic circuits. An alternative method utilizes a single excitation voltage signal containing several frequencies with known magnitudes and phases, such as a square wave. The impedance at each harmonic of the signal can be determined by analyzing the resulting magnitudes and phases of the measured current. The main drawback of this approach is that the amplitude of harmonics decreases significantly with frequency (proportional to $1/n$ for a square wave), leading to a reduced signal-to-noise ratio. In 1999, Searle proposed a method to assess impedance at multiple frequencies simultaneously by applying a digitally constructed multisinusoidal waveform [24]. This method demonstrated advantages over the square wave approach and proved feasible for monitoring impedance changes due to temporal evolution of the skin-electrode interface within a frequency range pertinent to electrodermal activity (10 Hz - 1000 Hz) at a rate of 0.3 spectra per second. The required setup included a personal computer, a data acquisition board, and an impedance frontend for signal conditioning and digital processing. In 2013, Sanchez et al. introduced a similar method based on multisinusoidal waveform excitation. Their approach aimed to achieve higher temporal resolution in impedance spectroscopy (124 spectra per second) over a broader frequency range (1 kHz - 939 kHz), utilizing a comparable setup [25]–[27]. More recent advancements, such as those by Santoso et al. [28], have focused on reducing the size of BIA systems while increasing acquisition rates. They achieved a full spectrum of 54 frequencies ranging from 100 Hz to 100 kHz in under one minute. Ruiz-Vargas et al. [29] developed a more compact system capable of capturing spectra at 5 frequencies between 1 kHz and 1 MHz in just 200 ms. Xuanjie Ye et al. introduced a highly promising device that combines multisine excitation for low frequencies (< 1 kHz) and signal tones for higher frequencies, enabling a scan of 28 frequencies in just 460 ms [30]. These powerful systems demonstrate significant progress in bioimpedance spectroscopy towards more portable, compact, and fast devices. However, none of them manage to integrate all of these features: a compact, wrist-worn form factor, a rapid acquisition rate with more than 5 spectra per second across a sufficient range of frequencies, along with embedded signal processing and wireless communication capabilities. In the context of EDA measurements, we developed a method based on a multisinusoidal waveform aimed at providing impedance values continuously. This method is also adaptable to portable systems, enabling in-situ EDA assessment during experiments with freely-moving participants, as described in the following section.

B. Application to electrodermal activity

The proposed method to achieve impedance spectroscopy continuously consists in injecting a current (or applying a

voltage) based on a multi-sinusoidal waveform, containing a finite number of frequencies of equal amplitude in the range of interest. Following the sampling of both current and voltage across the electrodes, a digital analysis is then performed, starting with the computation of the Fast Fourier Transform of the signals. Since the signals were sampled synchronously, the complex values of the result can be divided to obtain real and imaginary parts of the impedance, specifically from the frequency intervals (termed "bins") of the FFT that contain the frequencies composing the original waveform. This processing can be applied on a sliding window at a sufficient rate (i.e. faster than a rate of 5 Hz) to obtain a time varying signal for real and imaginary parts of the impedance at each frequency.

For the resulting impedance values to be accurate enough for subsequent analysis of SCL and SCRs, the digital processing must fulfill the following conditions:

- The sampling rate should be high enough to acquire precisely the highest frequency composing the multi-sinusoidal waveform. Usually, a sampling rate ten times higher than this frequency can be considered sufficient;
- The length of the sliding window should be large enough to contain several periods of the lowest frequency so that the FFT results remain accurate at lower frequencies;
- The number of points for computing the FFT, together with the difference between two consecutive frequencies composing the waveform, must be high enough so that each of its bins never contains more than one of these frequencies. Indeed, the number of points N used for the FFT and the sampling rate, F_s , determine the width of the bins, Δf , according to (1).

$$\Delta f = F_s / N \quad (1)$$

Another strong limitation involves the waveform amplitude, as it consists of a sum of sinusoidal signals. The total amplitude of the generated waveform increases with the number of frequencies. Whether applied as a current or as a voltage, this signal should remain within a limited amplitude range so that the total injected current does not exceed $20 \mu\text{A}$ and the voltage remains of the order of a volt [17], [31]. Therefore, a compromise between the number of frequencies composing the waveform and the respective amplitude of the signal at each frequency must be found. However, this trade-off can be optimized by properly adjusting the phase difference between all of the frequencies. We found that a good way to obtain a homogeneous envelop of the waveform over time is to select the best signal among multiple generations using random phases for each frequency. The criterion used for this selection is the maximum resulting amplitude of each frequency after normalisation of the waveform.

Finally, the performance of this method will essentially rely on the electronic components chosen for the generation, acquisition, processing, and transmission of the signals. First, the quality of the waveform will depend on the resolution and rate of the digital to analog converter, and then the analysis quality will essentially depend on the sampling rate as well as the rate at which voltage and current FFTs are computed.

To illustrate this method, we developed a dedicated wearable device capable of performing impedance spectroscopy continuously during in-situ experiments. Due to constraints inherent to embedded devices, namely size, power consumption and wireless communication, the device presented in the next section represents an optimized trade-off between computing power and signal quality.

III. IMPLEMENTATION OF REAL-TIME IMPEDANCE SPECTROSCOPY ON A WEARABLE DEVICE

A. Electronic architecture

To demonstrate the feasibility of implementing continuous impedance spectroscopy for EDA, we designed a wearable device primarily centered around two integrated circuits.

The CY8C4A45PVI-481 (Infineon Technologies AG) is a programmable analog coprocessor from the Programmable System on Chip (PSoC) family. This coprocessor is used for the generation of the multi-sinusoidal waveform, as well as conditioning the resulting voltage and current signals preceding their sampling. Further details regarding the generation of the waveform and signal conditioning with this component are provided in section III-C.

The nRF52840 (Nordic Semiconductor) is a system-on-chip which integrates a 32-bit ARM Cortex-M4 CPU with a floating-point unit running at 64 MHz, and a 2.4 GHz wireless transceiver compatible with Bluetooth Low Energy. This component is well known for its remarkably low power consumption across all its available functionalities. The acquisition, processing of signals, and transmission of impedance values carried out by this component are described in section III-D.

Additionally, our design includes a 150 mAh Lithium-Polymer battery and power management through the usage of dedicated integrated circuits, as well as an on-off switch and LED indicators. The overall electronic design results in a 3.65 cm x 2.6 cm circuit board size which is convenient for a wrist-worn device (Figure 1).

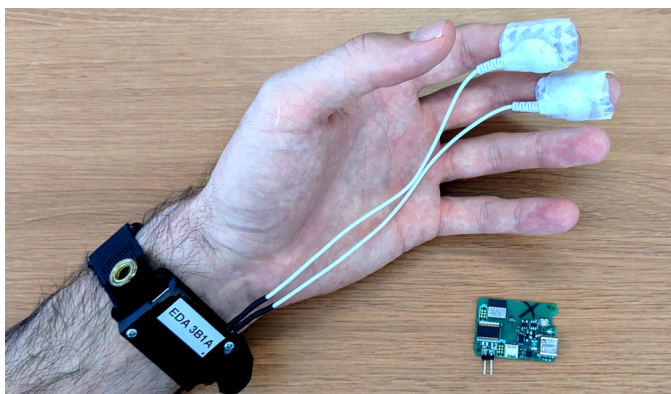


Fig. 1. Picture of the electronic device worn on the wrist, connected to two electrodes placed on the distal phalanges of the index and middle fingers. The image also shows the printed circuit board removed from its plastic housing.

B. Parameter adjustment

Parameter adjustment for the waveform and sampling rates, as well as the FFT window length and update rate, mainly

depends on the available computing power. In our case, to maximize all these parameters, we implemented internal hardware mechanisms for clock generation and dual-channel ADC sampling. Additionally, for the FFT calculation, we take advantage of the hardware floating-point unit and the CMSIS DSP library which offers optimized FFT computation. Thus, we obtained the following maximum rates:

- DAC and ADC sampling rates of 4096 Hz;
- FFT sliding window length of 2048 points (i.e. 0.5 s);
- FFT sliding window step of 512 points (i.e. 0.125 s) which implies that impedance values at each frequency are computed at a rate of $4096/512 = 8$ Hz.

This parametrisation is a compromise between duration of FFT calculation, based on the window length, and the update rate.

C. Signal generation

Our method consists in using a 16-frequency multi-sinusoidal waveform that encompasses the frequencies of interest (Table I). In our implementation, this signal is injected through the electrodes using two software-controlled current sources (IDAC [32]), integrated in the PSoC component. The first one is a current source which can push current out (positive current source) and the second one is a current sink which can pull current in (negative current source). Both are used to generate the positive and negative half of the waveform.

The 0 to 4.76 μA range was selected to prevent the signal from exceeding the 10 $\mu\text{A cm}^{-2}$ density limit, as recommended in the literature to prevent electrical nonlinearities in the skin [31], [33]. These sources are software-controlled within the PSoC using an unsigned 7-bit value, thus forming together a signed 8-bit digital-to-analog current converter with a maximal current amplitude of 9.52 μA . The firmware programmed into the PSoC contains data of the waveform generated beforehand, as well as a pin-based interrupt mechanism to update the current source values. This mechanism enables the use of an external clock to control the signal update rate. In our application, this benefits the sampling process carried out by the nRF52 MCU, which internally synchronizes the generation of a clock as well as ADC triggers for both voltage and current measurement.

From previous impedance measurements carried out with a reference instrumentation, the set of 16 frequencies listed in Table I was selected. We paid particular attention to ensure that these frequencies, in addition to being regularly distributed over the range 10 – 1000 Hz, meet two conditions:

- The first one is that all 16 frequencies are multiples of two, so that they are centered in the FFT bins whose width is 2 Hz according to (1);
- The second is that none of the frequencies are multiples of another. This condition prevents, if there are nonlinearities, harmonics generated during the measurement from overlapping with other frequencies.

The waveform was generated using Matlab software (The Mathworks). The process to select the final waveform was the following:

TABLE I
LIST OF THE 16 FREQUENCIES COMPOSING THE GENERATED WAVEFORM (IN HERTZ)

f_1	f_2	f_3	f_4	f_5	f_6	f_7	f_8
12	28	32	36	44	68	84	108
f_9	f_{10}	f_{11}	f_{12}	f_{13}	f_{14}	f_{15}	f_{16}
136	196	256	324	400	484	576	726

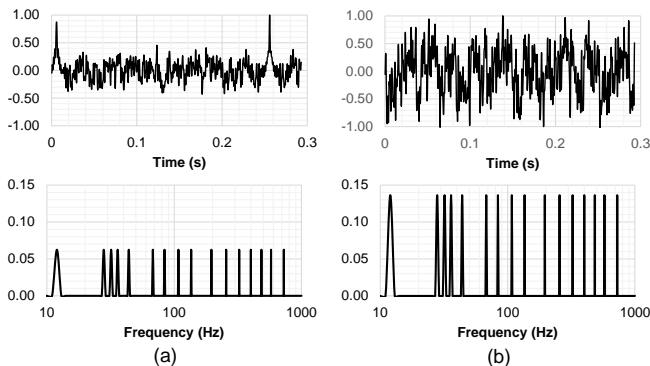


Fig. 2. Time and frequency representation of a waveform generated with synchronous cosines (a) compared to the selected waveform (b).

- 100,000 different waveforms of 4096 points with a $\Delta t = 1/4096$ s were computed by summing the 16 frequencies using equal amplitudes but randomly generated phases;
- Each waveform was individually normalized by dividing the waveform's values by the maximum absolute value of this particular waveform;
- A FFT was computed for each waveform to obtain the normalized amplitude of the component frequencies;
- The waveform having the highest normalized amplitude for the frequencies was selected.

This process ensures that phases for all frequencies are distributed so that each individual frequency retains the highest possible amplitude to maximize signal-to-noise ratio. Figure 2 illustrates the difference between a waveform generated using a sum of cosines for the 16 frequencies with null phase (i.e. worst possible case) and the waveform selected using the process described above (best case out of the 100,000 generated signals). The figure shows the FFT of both signals to enable the comparison of the amplitude of each frequency. We can see that for the sum of cosines, after signal normalisation, we obtain an individual amplitude for each frequency of 0.0625. However, using our generation and selection method, we obtain individual amplitudes of 0.136 for each frequency after signal normalisation. For a resulting injected current with a maximum amplitude of $4.76 \mu\text{A}$, we obtained with this method an amplitude of $0.647 \mu\text{A}$ for each frequency, instead of $0.297 \mu\text{A}$ if simple cosines would have been used.

Even if the current generated is known (by knowing the range of the current source and the waveform data), the actual current injected through the electrodes is also measured, in addition to the generated voltage across the electrodes. For current measurement, a transimpedance amplifier is formed by using one of the operational amplifiers integrated within the PSoC, along with an external gain resistor. Also, a second

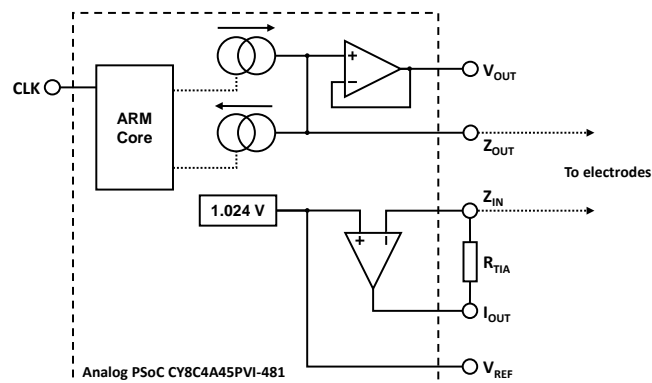


Fig. 3. Electronic circuit built with the programmable analog components of the PSoC to form the measurement frontend.

integrated operational amplifier is used as a voltage follower to buffer the difference of potential across the electrodes. Figure 3 illustrates the complete frontend for the waveform generation and signal conditioning before acquisition. Output V_{OUT} is the difference in potential across the electrodes referenced to V_{REF} (1.024 V). The software-controlled current sources inject current to the electrodes from Z_{OUT} to Z_{IN} . The current measured is converted to voltage using a transimpedance amplifier with a gain resistor R_{TIA} of 220 k Ω . The outputs I_{OUT} , V_{OUT} , and V_{REF} are then connected to ADC inputs of the nRF52840 to sample voltage and current signals synchronously with waveform generation (CLK input).

D. Acquisition, processing and transmission

Sampling of current and voltage, as well as signal processing for frequency analysis and impedance calculation, are carried out by the nRF52840. A 4096 Hz clock is generated using an internal timer to trigger updates of the waveform with the PSoC. Using an internal mechanism called a Peripheral Programmable Interconnect (PPI), current and voltage signals are sampled synchronously with this clock at an identical rate. Every 512 samples, an interrupt is triggered and the two sliding windows (one for each signal) of 2048 points are updated. A FFT is then computed on both windows giving real and imaginary values of voltage and current for each bin of the FFT. Finally, the 16 complex values of the voltage FFT corresponding to the frequencies of the waveform are divided by their respective values of the current FFT. A numerical gain is applied to compensate for the TIA gain, thereby obtaining the complex impedance at each of the 16 frequencies. Real and imaginary values of impedances are stored in single-precision floating format and sent over Bluetooth Low Energy to the host. Figure 4 illustrates the signal processing chain.

A simple graphical user-interface was developed to control Bluetooth connection, real-time visualisation of Nyquist and Bode plots, and file storage on any device equipped with Bluetooth Low Energy. Figure 5 is a screenshot of a section of the application which plots in real-time the module of the impedance of each of the 16 frequencies acquired simultaneously at a rate of 8 samples per frequency per second. This illustrates the occurrence of SCRs on the measured signal,

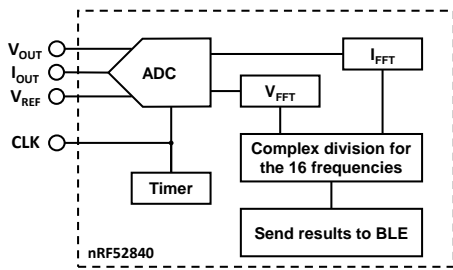


Fig. 4. Flowchart of signal acquisition and processing in the nRF52840 for calculation of impedance at each of the 16 frequencies composing the waveform.

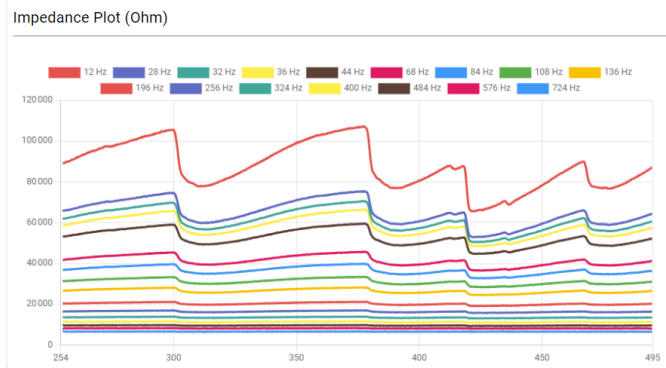


Fig. 5. Section of the software developed to show the impedance module of each of the 16 frequencies acquired simultaneously during electrodermal activity measurements. The plot is refreshed in real-time in the application at a rate of 8 times per second per frequency.

especially on the lowest frequency (12 Hz) as it shows the highest impedance magnitude. Figure 6 is a screenshot of another section of the desktop application which fits in real time the data collected to a single Cole element equivalent circuit. The data are plotted on a Nyquist plot, a parametric graph where the real part of impedance is on the x-axis and the imaginary part on the y-axis. In this plot, the single Cole-element equivalent circuit appears as a circular shape (indicated by the dashed line), with dots representing impedance values at 16 frequencies within this plane.

IV. EVALUATION OF THE MEASUREMENT QUALITY

Two experiments were conducted to assess whether this implementation of our method could enhance the measurement and analysis of EDA. In order to evaluate its accuracy, the device was tested first against static, discrete impedance circuits with known values. Secondly, the device was compared to a reference instrument dedicated to bioimpedance spectroscopy, to evaluate the behaviour of the device with real skin-electrode interfaces and living tissue. Pearson correlation coefficient [34] as well as Bland-Altman analysis [35] were run to compare and discuss, for both experiments, the measurements obtained against theoretical values and the reference instrument.

A. In-vitro evaluation of discrete impedance

For in-vitro evaluation, the device was tested on different circuits composed of discrete resistors and capacitors. These components were mounted on small milled circuit boards to

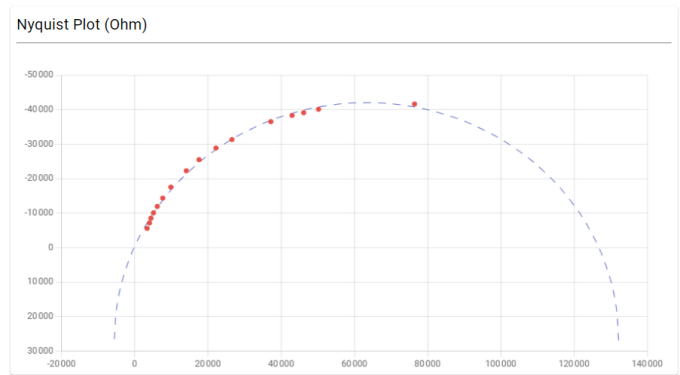


Fig. 6. Section of the software developed to show the instant Nyquist plot (imaginary part vs. real part of the impedance). The points correspond to the 16 frequencies acquired simultaneously. The dashed line represents an instant fit of the data to a circular model, equivalent to a single Cole-element circuit. The application allows real-time monitoring of the Nyquist diagram variations.

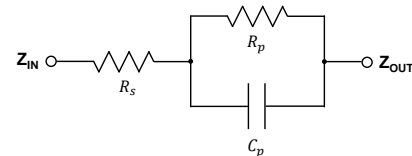


Fig. 7. Schematic of the test circuit used for in-vitro evaluation of the device

ensure the shortest tracks between components and minimal parasitic capacitance. The impedance model chosen for in-vitro testing is a simple one-relaxation time constant circuit composed of one resistance, R_s , in series with a second resistance, R_p , in parallel with a capacitance, C_p , as shown on Fig. 7. This circuit is equivalent to a complex impedance, represented by (2).

$$Z = R_s + \frac{R_p}{1 + j\omega R_p C_p} \quad (2)$$

This test circuit is a simplified version of the equivalent circuit models often used to represent measured skin impedances over the frequency range 10 – 1000 Hz. However, the objective of this experiment is not to reproduce realistically the electrical behaviour of the skin, but rather to produce impedance values typically observed when measuring EDA on palms. To select various values for the three components, impedance spectroscopy measurements were performed on 6 voluntary subjects using the MFIA Impedance Analyzer (Zurich Instruments) in a 2-electrode configuration. The electrodes used were Softrace small-sized electrodes (ConMed), placed on distal phalanges of index and middle fingers on the non-dominant hand, 5 minutes prior to the measurement. The data collected were fitted into ZView software (Scribner LLC) using the equivalent electrical circuit previously described, in order to obtain values for R_s , R_p and C_p . Six test circuits (C1 to C6) were built using 1% precision film SMD resistors and 1% precision C0G/NP0 SMD capacitors. The values of all components used were also precisely measured before the assembly of the circuits using a U1732C LCR meter (Keysight) and are listed in Table II. Having precise values

TABLE II

LIST OF COMPONENTS VALUES FOR THE 6 TEST CIRCUITS

	C1	C2	C3	C4	C5	C6
R_s (Ω)	2100	1500	2492	2400	2609	2318
R_p (Ω)	45299	68031	64901	88872	105037	86569
C_p (nF)	151.2	47.3	181.8	146.7	94.5	99.2

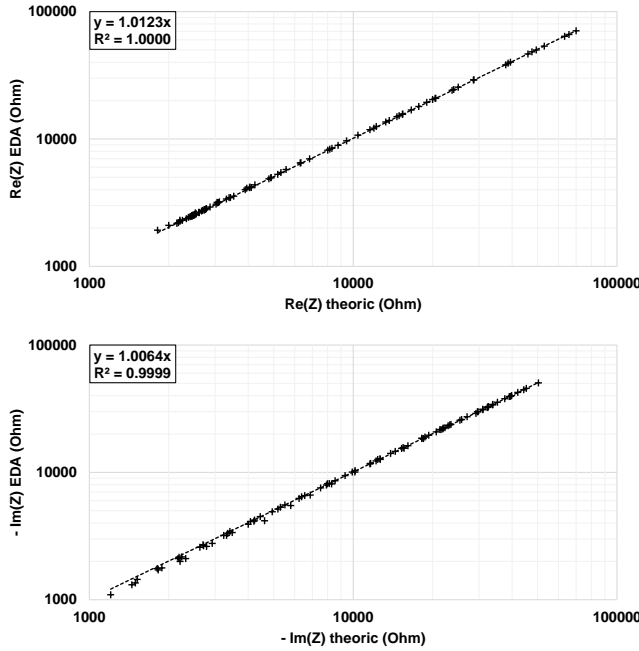


Fig. 8. Correlation plots of real and imaginary parts for all impedances obtained during in-vitro measurements. X-axis represents the theoretical real ($\text{Re}(Z)$ theoretic) and imaginary ($\text{Im}(Z)$ theoretic) parts of the impedance. Y-axis represents the real and imaginary part of the impedance measured with the device. For each dataset the linear approximation has been plotted and the equation as well as the Pearson's coefficient of determination (R^2) are shown.

for these components enabled us to calculate theoretically the real and imaginary values of the equivalent impedance Z at the 16 angular frequencies $\omega = 2\pi f$ measured, according to (3) and (4).

$$\text{Re}(Z) = R_s + \frac{R_p}{1 + R_p^2 C_p^2 \omega^2} \quad (3)$$

$$\text{Im}(Z) = \frac{-R_p^2 C_p \omega}{1 + R_p^2 C_p^2 \omega^2} \quad (4)$$

Figure 8 shows the correlation plot between measurements made with our device and the calculated impedances for each circuit using (3) and (4), based on the components' value measured with the LCR meter. Two plots were made to separate real and imaginary part of the impedance. However, when comparing two methods of measurement, a Bland-Altman is a more suitable tool as it allows for the visualization of the agreement between the two methods and any systematic bias or random error.

Figure 9 shows Bland-Altman plots as well as the limits of agreement (± 1.45 interquartile range) for the real (upper plot) and imaginary (lower plots) part of the impedance of the

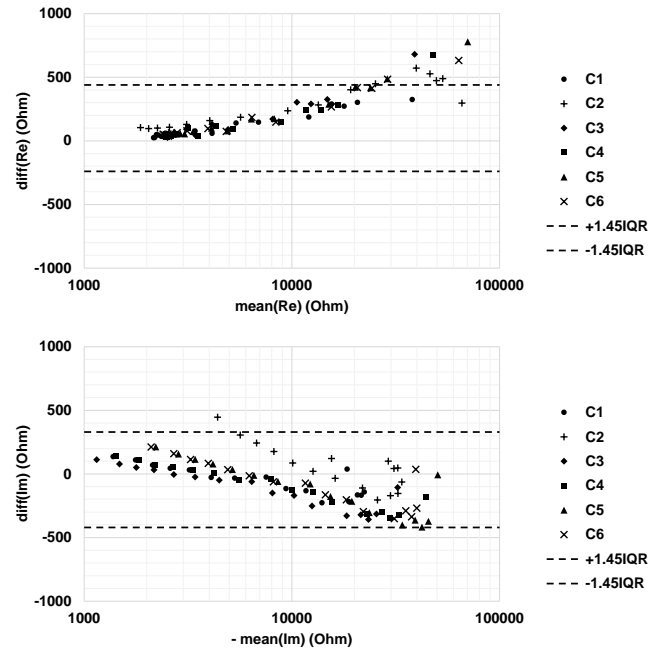


Fig. 9. Bland-Altman plots of real and imaginary parts of the impedance for the measurements made on electrical circuits. Y-axis is the difference between the value measured with the device and the theoretical value calculated from the values of the circuit components. X-axis is the mean of both values.

TABLE III

ERRORS OF MEASUREMENT ON STATIC TEST CIRCUITS

	Real part		Imaginary part	
	Absolute (Ω)	Relative (%)	Absolute (Ω)	Relative (%)
f_1	564	1.1	-17	0.3
f_2	395	1.6	-221	0.8
f_3	351	1.7	-264	0.9
f_4	368	2.0	-231	0.9
f_5	271	1.7	-279	1.1
f_6	183	1.9	-242	1.4
f_7	190	2.7	-173	1.1
f_8	95	1.5	-157	1.3
f_9	117	2.7	-65	0.6
f_{10}	80	2.2	-47	0.7
f_{11}	66	2.1	-9	0.3
f_{12}	60	2.2	35	0.7
f_{13}	53	2.1	78	1.9
f_{14}	53	2.3	110	3.2
f_{15}	55	2.4	153	5.5
f_{16}	53	2.4	210	9.4

circuits C1 to C6 at each of the 16 frequencies. For clearer visualisation, the axes are displayed using a logarithmic scale so that the data are more evenly spaced across the graphs.

Table III lists the averaged absolute errors $\bar{\Delta x}$ and the averaged relative errors $\bar{\Delta x}/x$ obtained for real and imaginary values of the impedance at each frequency.

Also, the measurements obtained using our device on each of the 6 circuits for the 16 frequencies were fitted using ZView software to predict R_s , R_p and C_p which were then compared to the components' value measured with the LCR meter. Table IV lists averaged absolute and relative errors for the fitted component values against values measured with the

TABLE IV
ERRORS IN FITTING ON STATIC TEST CIRCUITS

	Absolute	Relative
R_s	60 Ω	3.4 %
R_p	307 Ω	0.1 %
C_p	0.7 nF	0.5 %

LCR meter.

B. In-vivo evaluation

The second experiment aims at comparing our device with a reference instrumentation when performing impedance spectroscopy for EDA on a human subject. For this experiment, the reference instrumentation used was the Medical Research ISX-3 from Sciospec. Compared to the MFIA, the software provided with the ISX-3 enables selecting a list of fixed frequencies rather than an automated selection of frequencies based on a given range and sweep mode (logarithmic or linear). Hence, we were able to measure impedances at the exact same 16 frequencies as our device to compare measurement results. This experiment is very challenging to set up in order to obtain comparable results between both instrumentations. Ideally, measurements from the two instruments should be made at the same time, on the same body site with the same electrodes, and for the same duration. This is mainly because EDA is a constantly varying signal, so measurements have to be made simultaneously. Additionally, having different electrodes or measuring on different body sites would inevitably lead to a variation in the electrode-skin interface impedance.

We followed a protocol aiming at minimizing EDA as well as preventing variations due to the electrode-skin interface in order to compare our device with the ISX-3 impedance analyser. This protocol has been formerly reviewed and approved by a local ethics review board. The experiment was run on 7 voluntary and healthy subjects (S1 - S7) who were notified concerning the objectives and conditions of the experiments and signed an informed consent form. The experiment took place after lunch, with the intention of carrying out measurements during postprandial sleepiness. Each subject was equipped with ConMed Softrace small-sized electrodes placed on the distal phalanges of their index and middle fingers on the non-dominant hand. Then they were instructed to lie down on a bed and rest for 30 minutes in a dark and silent room. Using this protocol, we expected the subject to fall asleep, thus reducing EDA to a minimal level. This is necessary to facilitate meaningful comparison between both instruments, as while our device can perform 8 measurements per second at each frequency, it takes about 85 seconds with the ISX-3 to obtain a full impedance spectrum. Consequently, a high probability remains that a SCR occurs during this period. Cables attached to the electrodes were connected to the measurement instruments located in an adjoining room, so that the subject could not hear the experimenter. Initially, cables were connected to our device and the signal is continually monitored by the experimenter. By visual inspection, the experimenter can then evaluate when electrodermal activity is significantly low, and then disconnect the cables from our device to connect

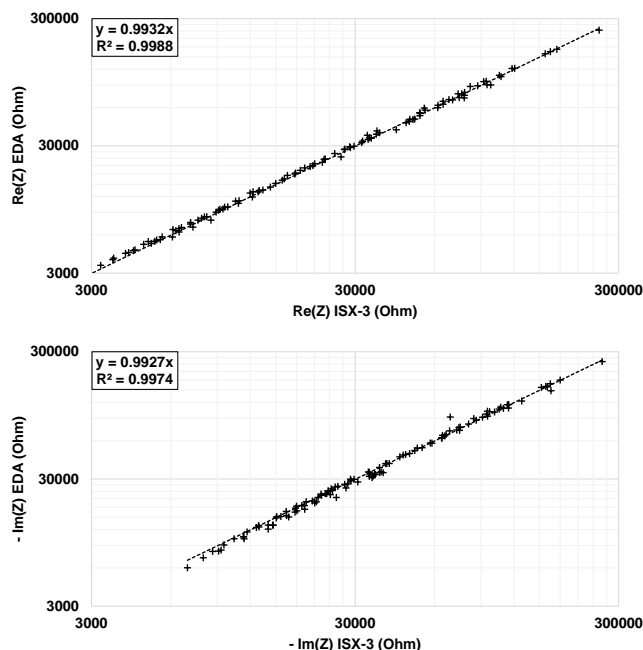


Fig. 10. Correlation plots of real and imaginary parts for all impedances obtained during in-vivo measurements. X-axis represents real and imaginary parts of the impedance measured with the ISX-3. Y-axis represents real and imaginary parts of the impedance measured with the device. For each dataset the linear approximation has been plotted and the equation as well as the Pearson's coefficient of determination (R^2) are shown.

them to the ISX-3. A single set of measurement of the complex impedance at each of the 16 frequencies was performed and data were saved before reconnecting our device. Data collected with the ISX-3 device were compared to values collected by our device just after the measurement.

Figure 10 shows the correlation plot between measurements made with our device and those consecutively made with the ISX-3. Two plots were made to separate real and imaginary part of the impedance. Figure 11 shows Bland-Altman plots as well as the limits of agreement (± 1.45 interquartile range) for the real (upper plot) and imaginary (lower plots) part of the impedance of the subjects S1 to S7 at each of the 16 frequencies. Table V reports absolute and relative differences between both devices.

V. DISCUSSION

Results obtained during both the *in vitro* and *in vivo* experiments confirm the ability of our method to perform impedance spectroscopy for the analysis of EDA at a rate of 8 spectrums per second for 16 simultaneous frequencies. The constraints we imposed on the design of our device (wearable, low-power) gave inherent limits to this implementation such as window length and update rate, for the microcontroller to be able to compute voltage and current FFTs. Nonetheless, the in-vitro results obtained under static conditions provided precise results at most frequencies. All relative errors on the real part were below 3%. As for the imaginary part, the relative error remains mostly below 3%, except for the 3 highest frequencies. The notable trend observed in the absolute

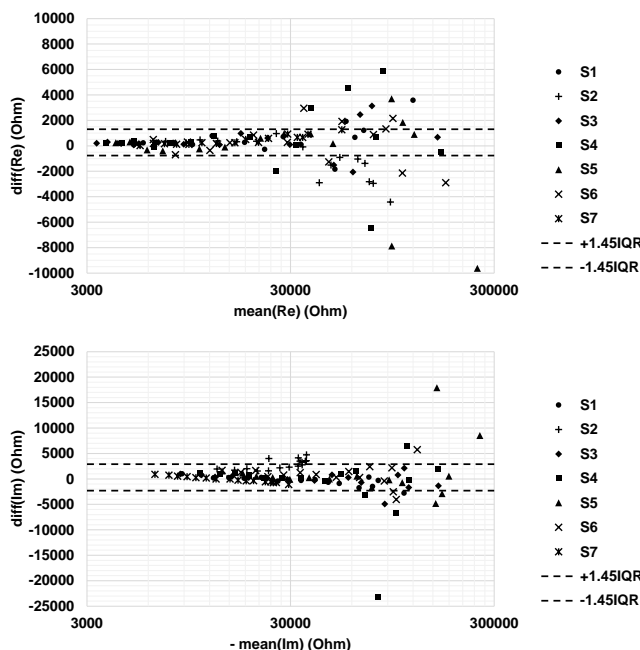


Fig. 11. Bland-Altman plots of real and imaginary parts of the impedance for the measurements made during the in-vivo experiment. Y-axis is the difference between the value measured with the device and the value measured with the ISX-3. X-axis is the mean of both values.

TABLE V

DIFFERENCES IN MEASUREMENT DURING IN-VIVO EVALUATION

	Real part		Imaginary part	
	Absolute (Ω)	Relative (%)	Absolute (Ω)	Relative (%)
f_1	-1696	2.3	2131	4.6
f_2	991	3.2	327	3.0
f_3	803	2.2	621	3.8
f_4	-331	3.5	-793	3.6
f_5	-843	4.1	-1164	9.8
f_6	712	2.5	39	3.2
f_7	-26	2.2	618	2.3
f_8	31	5.2	570	2.5
f_9	290	1.6	320	1.7
f_{10}	512	3.5	396	1.8
f_{11}	183	2.3	639	2.3
f_{12}	139	2.7	436	2.1
f_{13}	100	3.4	608	3.4
f_{14}	74	5.7	905	5.4
f_{15}	242	4.6	1071	7.8
f_{16}	189	4.4	1332	11.6

error for both real and imaginary parts suggests a systematic bias in the measurements specific to our electronic design. This warrants further investigation to improve the accuracy of the device (parasitic capacitance or resistance within the system or numerical errors during FFT and impedance computations). Currently, the non-negligible relative error in the imaginary part for the highest frequencies only have a substantial impact on the evaluation of the R_s value (average relative error of 3.4%), while its impact on R_p and C_p is negligible (average relative errors of 0.1% and 0.5% respectively). As for the in-vivo evaluation results, it must be emphasized that it is very difficult to obtain two identical measurement results, even from the same instrumentation, when assessing bioelectrical signals

on living tissues. Thus, we found the results obtained from our device particularly satisfactory when compared to the ISX-3 device. This also confirms that our protocol appears well-suited for the comparison of two instrumentations performing impedance spectroscopy applied to EDA. Moreover, the ISX-3 device exhibited significant variability when measuring at 44 Hz, which explains the larger differences observed at this frequency between the two devices. This may likely be attributed to 50 Hz power lines interference which affects this device. Additionally for subject S2, a greater disparity between the two plots obtained can be explained by the significant EDA of this subject. This made it very difficult for the experimenter to find an appropriate time for connecting the ISX-3, and it is very likely that a SCR occurred during the ISX-3 measurement. The larger differences found for the imaginary part at higher frequencies seem to confirm the existence of the systematic bias already highlighted by the in-vitro experiment.

VI. CONCLUSION

In this paper, a method of continuous impedance spectroscopy was presented to assess electrodermal activity (Section II.B and III). The parametrization advantages of this method render it suitable for implementation across various platforms. The example proposed in this paper is a wearable device constrained by specific factors such as embedded processing, device size, and autonomy. This device demonstrated the performance of this method which extends the way EDA is measured with traditional methods using DC current or AC current at a single frequency. As shown on Figures 5 and 6, this method opens new avenues of research regarding modelling of EDA through the study of the underlying electrical model. In particular, this approach makes possible the fitting of measured impedances to different topologies of equivalent circuits, containing one or several relaxation time constants / dispersions [3, p. 51], to better differentiate what is specific to the activity of sweat glands, and what pertains to the impedance of the electrode-skin interface (effects of the skin's hydration [15], [24]). To the best of our knowledge, time variations of Cole-Cole equation's parameters have not been studied in the context of EDA at a such rate (8 samples per second). This type of analysis will be utilized in future studies to assess its potential contribution to the repeatability and comparability of different in-vivo experiments, as well as to evaluate the possibility of making skin conductivity measurements more robust for electrodermal activity analysis.

REFERENCES

- [1] L. C. Johnson and A. Lubin, "Spontaneous electrodermal activity during waking and sleeping," *Psychophysiology*, vol. 3, no. 1, pp. 8–17, 1966.
- [2] W. Boucsein, *Electrodermal Activity*. Boston, MA: Springer US, 2012.
- [3] O. G. Martinsen and A. Heiskanen, *Bioimpedance and bioelectricity basics*. Elsevier, 2023.
- [4] J. N. Langley, "The autonomic nervous system," *Brain*, vol. 26, no. 1, pp. 1–26, 1903.

- [5] K. Kasos, S. Zimonyi, B. Gonye, *et al.*, “Obimon: An open-source device enabling group measurement of electrodermal activity,” *Psychophysiology*, vol. 56, no. 8, e13374, 2019.
- [6] R. Zangróniz, A. Martínez-Rodrigo, J. M. Pastor, M. T. López, and A. Fernández-Caballero, “Electrodermal activity sensor for classification of calm/distress condition,” *Sensors*, vol. 17, no. 10, p. 2324, 2017.
- [7] A. Nakasone, H. Prendinger, and M. Ishizuka, “Emotion recognition from electromyography and skin conductance,” in *Proc. of the 5th international workshop on biosignal interpretation*, Citeseer, 2005, pp. 219–222.
- [8] J. Tarchanoff, “Galvanic phenomena in the human skin during stimulation of the sensory organs and during various forms of mental activity,” *Pflügers Archiv für die gesammte Physiologie des Menschen und der Tiere*, vol. 46, pp. 46–55, 1890.
- [9] C. L. Lim, C. Rennie, R. J. Barry, *et al.*, “Decomposing skin conductance into tonic and phasic components,” *International Journal of Psychophysiology*, vol. 25, no. 2, pp. 97–109, 1997.
- [10] M. Benedek and C. Kaernbach, “A continuous measure of phasic electrodermal activity,” *Journal of neuroscience methods*, vol. 190, no. 1, pp. 80–91, 2010.
- [11] C. Fere, “Note on changes in electrical resistance under the effect of sensory stimulation and emotion,” *Comptes rendus des seances de la société de biologie*, vol. 5, pp. 217–219, 1888.
- [12] O. Pabst, C. Tronstad, S. Grimnes, D. Fowles, and Ø. G. Martinsen, “Comparison between the ac and dc measurement of electrodermal activity,” *Psychophysiology*, vol. 54, no. 3, pp. 374–385, 2017.
- [13] S. Grimnes, A. Jabbari, Ø. G. Martinsen, and C. Tronstad, “Electrodermal activity by dc potential and ac conductance measured simultaneously at the same skin site,” *Skin Research and Technology*, vol. 17, no. 1, pp. 26–34, 2011.
- [14] D. C. Fowles, M. J. Christie, R. Edelberg, W. W. Grings, D. T. Lykken, and P. H. Venables, “Publication recommendations for electrodermal measurements,” *Psychophysiology*, vol. 18, no. 3, pp. 232–239, 1981.
- [15] E. McAdams, “Bioelectrodes,” in *Encyclopedia of Medical Devices and Instrumentation*. John Wiley & Sons, Ltd, 2006, ISBN: 9780471732877.
- [16] C. Tronstad, G. K. Johnsen, S. Grimnes, and Ø. G. Martinsen, “A study on electrode gels for skin conductance measurements,” *Physiological Measurement*, vol. 31, no. 10, pp. 1395–1410, Oct. 1, 2010.
- [17] Society for Psychophysiological Research Ad Hoc Committee on Electrodermal Measures, “Publication recommendations for electrodermal measurements,” *Psychophysiology*, vol. 49, no. 8, pp. 1017–1034, Aug. 2012.
- [18] H. F. Posada-Quintero and K. H. Chon, “Innovations in electrodermal activity data collection and signal processing: A systematic review,” *Sensors*, vol. 20, no. 2, p. 479, Jan. 15, 2020.
- [19] C. Tronstad, M. Amini, D. R. Bach, and Ø. G. Martinsen, “Current trends and opportunities in the methodology of electrodermal activity measurement,” *Physiological Measurement*, vol. 43, no. 2, Feb. 28, 2022.
- [20] A. Böhm and B. L. Heitmann, “The use of bioelectrical impedance analysis for body composition in epidemiological studies,” *European Journal of Clinical Nutrition*, vol. 67, S79–S85, S1 Jan. 2013.
- [21] U. G. Kyle, I. Bosaeus, A. D. De Lorenzo, *et al.*, “Bioelectrical impedance analysis-part II: Utilization in clinical practice,” *Clinical Nutrition*, vol. 23, no. 6, pp. 1430–1453, Dec. 2004.
- [22] U. Kyle, “Bioelectrical impedance analysis-part I: Review of principles and methods,” *Clinical Nutrition*, vol. 23, no. 5, pp. 1226–1243, Oct. 2004.
- [23] L. Mørkrid and Z. Qiao, “Continuous estimation of parameters in skin electrical admittance from simultaneous measurements at two different frequencies,” *Medical and Biological Engineering and Computing*, vol. 26, pp. 633–640, 1988.
- [24] A. Searle and L. Kirkup, “Real time impedance plots with arbitrary frequency components,” *Physiological measurement*, vol. 20, no. 1, p. 103, 1999.
- [25] B. Sanchez, E. Louarroudi, E. Jorge, J. Cinca, R. Bragos, and R. Pintelon, “A new measuring and identification approach for time-varying bioimpedance using multisine electrical impedance spectroscopy,” *Physiological measurement*, vol. 34, no. 3, p. 339, 2013.
- [26] B. Sanchez, E. Louarroudi, R. Bragos, and R. Pintelon, “Harmonic impedance spectra identification from time-varying bioimpedance: Theory and validation,” *Physiological measurement*, vol. 34, no. 10, p. 1217, 2013.
- [27] B. Sanchez, G. Vandersteen, I. Martin, *et al.*, “In vivo electrical bioimpedance characterization of human lung tissue during the bronchoscopy procedure. a feasibility study,” *Medical Engineering & Physics*, vol. 35, no. 7, pp. 949–957, 2013.
- [28] D. R. Santoso, B. Pitaloka, C. S. Widodo, and U. P. Juswono, “Low-cost, compact, and rapid bio-impedance spectrometer with real-time bode and nyquist plots,” *Applied Sciences*, vol. 10, no. 3, 2020, ISSN: 2076-3417. DOI: 10.3390/app10030878. [Online]. Available: <https://www.mdpi.com/2076-3417/10/3/878>.
- [29] A. Ruiz-Vargas, J. W. Arkwright, and A. Ivorra, “A portable bioimpedance measurement system based on red pitaya for monitoring and detecting abnormalities in the gastrointestinal tract,” in *2016 IEEE EMBS Conference on Biomedical Engineering and Sciences (IECBES)*, 2016, pp. 150–154. DOI: 10.1109/IECBES.2016.7843433.
- [30] X. Ye, T. Jiang, Y. Ma, D. To, S. Wang, and J. Chen, “A portable, low-cost and high-throughput electrochemical impedance spectroscopy device for point-of-care biomarker detection,” *Biosensors and Bioelectronics: X*, vol. 13, p. 100301, 2023, ISSN: 2590-1370. DOI: <https://doi.org/10.1016/j.biosx.2022.100301>. [Online]. Available: <https://www.sciencedirect.com/science/article/pii/S2590137022001947>.

- [31] R. Edelberg, "Electrical properties of the skin," in *Methods in Psychophysiology*, C. C. Brown, Baltimore: Williams & Wilkins, 1967.
- [32] *PSoC 4 Current Digital to Analog Converter (IDAC7)*, 002-20200, Rev. 1.10, Infineon, Oct. 2017. [Online]. Available: <https://www.infineon.com/cms/en/design-support/tools/sdk/psoc-software/psoc-4-components/psoc-4-current-digital-to-analog-converter/>.
- [33] D. Salter, "Quantifying skin disease and healing in vivo using electrical impedance measurements," *Non-invasive physiological measurements*, vol. 1, pp. 21–64, 1979.
- [34] K. Pearson, "Notes on regression and inheritance in the case of two parents," *Proceedings of the royal society of London*, vol. 58, pp. 240–242, 1895.
- [35] J. M. Bland and D. G. Altman, "Statistical methods for assessing agreement between two methods of clinical measurement," *Lancet*, vol. 327, 8476 Feb. 1986.



Bertrand Massot received his PhD in Biomedical Engineering in 2011 at INSA Lyon, France. He is now an assistant professor at INSA Lyon within the Devices for Health and Environment group of the Lyon Institute of Nanotechnology. His research interests include the development of smart, wearable sensors for the continuous and long-term monitoring of biosignals at home and on the move. He is specialized in the design of on-board mixed-signal electronics and wireless sensors as well as embedded software

and interfaces. He develops novel portable instrumentations for the continuous assessment of the autonomic nervous system activity and led the development of a wireless body sensor network to assess cardiac, respiratory, thermal, electrodermal and physical activities for the continuous monitoring of health.



Emeric Desmazure received his Ms. degree in 2021 at the Faculty of Medicine of Nancy, France, in the field of biomedical engineering. He was involved in significant projects, including the study of cranial nerves through diffusion MRI at the CREATIS laboratory at INSA Lyon, France. He also contributed to research on sensory neuroprosthesis for the restoration of hearing and balance at the Western Switzerland University Cochlear Implants Center, Geneva University Hospitals, Switzerland. Since 2022,

he has been pursuing a PhD on the topic "Real-time impedance spectroscopy for the measurement of electrodermal activity" under the guidance of Dr. Bertrand Massot and Pr. Claudine Gehin within the Devices for Health and Environment group of the Lyon Institute of Nanotechnology at INSA Lyon, France.



Amalric Montalibet received his PhD in Electrical Engineering, Electronics, and Automation from INSA Lyon, France, in 2002. He also holds degrees in Electrical Engineering and Industrial Computing (1993), Physical Engineering with a focus on Instrumentation and Medical Imaging (1996), and an Advanced Studies Diploma in Biological and Medical Engineering (1997). In his early work, he pioneered tissue characterisation by combining bioelectrical impedance and ultrasound. He contributed to various biomedical projects in industry, including validating protocols for non-invasive ultrasound treatment of tumours, monitoring epileptic seizures, and designing clean rooms. Since 2015, Dr Montalibet has been a research engineer at INSA Lyon, actively contributing to bioelectrical impedance spectroscopy, medical applications, and sensor/electrode development at the Lyon Institute of Nanotechnologies.



Eric McAdams received his PhD in 1987 from Leeds University, Department of Medical Physics. Until 2020 he was at the Head of the Biomedical Sensors Group within the Nanotechnologies Institute of Lyon. Before that he was the Head of the Medical Sensors Group at NIBEC, University of Ulster and in 2001 he co-founded and was a director of a successful spin-out company from the University, Intelesens, pioneer in the area of wireless Vital Signs Monitoring. He is widely recognised as a leading specialist in the

study and modelling of the linear and non-linear electrical properties of materials and interfaces.



Claudine Gehin received the PhD degree in Applied Physics from the University of Savoie, Annecy, in 1998. She is currently Associate Professor with the National Institute of Applied Sciences, Lyon, France, and teaches electronics at the Department of Electrical Engineering. She joined the Nanotechnologies Institute of Lyon (INL - Institut des Nanotechnologies de Lyon - Biomedical Sensors Group) in 2003 to design and develop non-invasive biomedical sensors. Her research is focused on ambulatory, wear-

able sensors for the monitoring of thermal, neurophysiological, vascular and mechanical parameters. She participated in 78 scientific papers, conference papers, book chapters and participated in 4 patents.